Assessing anodic microbial populations and membrane ageing in a pilot microbial electrolysis cell

M. Isabel San-Martín[a], Ana Sotres[a], Raúl M. Alonso[a], Jordi Díaz-Marcos[b], Antonio Morán[a], Adrián Escapa[a,c,*]

[a] Chemical and Environmental Bioprocess Engineering Group, Natural Resources Institute (IRENA), Universidad de León, Avda. de Portugal 41, Leon 24009, Spain.

[b] Nanometric Techniques Unit, Scientific and Technical Centers of the University of Barcelona, Lluís Soléi Sabarís 1-3, E-08028 Barcelona, Spain.

[c] Department of Electrical Engineering and Automatic Systems, Universidad de León, Campus de Vegazana s/n, 24071 León, Spain.

* Corresponding author:

   Tel.: 0034 987295394

   E-mail: adrian.escapa@unileon.es   (A.Escapa)

Highlights

- Large-scale BES can lead to a vertical stratification of anode microbial communities.
- Shear stress is hampering the development of an anodic biofilm.
- Ion exchange capacity of the membrane is reduced as consequence of the biofouling.
- Membrane matrix is specially deteriorated at the top of the reactor.
- Hydrogen production is feasible in a MEC treating a complex substrate.

Abstract

First large-scale experiences of bioelectrochemical systems (BES) are underway. However, there is still little knowledge on how the different elements that integrate a BES behave in near real-life conditions. This paper aims at assessing the impact of long-term operation on the cation exchange membrane and on the anodic biofilm of two 16 L Microbial Electrolysis Cells (MEC) designed for hydrogen production and ammonia recovery from pig slurry. Membrane deterioration was examined by physical, chemical and microscopy techniques at different locations, revealing a strong attachment of microorganisms and a significant decay in membrane properties such as ion exchange capacity and thermal stability. Anode microbial communities did not show a dramatic shift in the eubacteria composition at different sampling areas, although the relative abundance of some bacterial groups showed a clear vertical stratification. After 100 days of continuous operation, MEC performance did not declined significantly maintaining ammonium transport rates and H_2 production rates of 15.3 $gN \cdot d^{-1} \cdot m^{-2}$ and 0.2 $LH_2 \cdot L^{-1}_{reactor} \cdot d^{-1}$ respectively.

Keywords: Bioelectrochemical system, Scaling-up, Cation exchange membrane, Waste valorization, Anodic biofilm.

1. Introduction

Bioelectrochemical systems (BES) represent a relatively novel technology with a wide range of potential applications, the most interesting of which (from a technoeconomical point of view) can be those that allow the production of hydrogen or other fuels by the valorization of waste streams [1]. During the past 15 years, BES have experienced an intense phase of research in many of the areas related to their development (materials, engineering and microbiology) that has paved the way for the first experiences at a pilot scale [2]. To further advance in the development of this technology, it is of utmost importance to have a clear understanding of how the different elements that integrate a bioelectrochemical reactor behave in near real-life conditions. Perhaps the (bio-)electrodes (anode and cathode) and the ion exchange membranes are the most crucial of these elements [3]. This is not only because they play a direct role in the basic bioelectrochemical processes that comprise the principle of operation of this technology, but also because they contribute significantly to the capital cost of BES [4] [5] [6].

Bioelectrodes rely on the ability of certain electroactive microorganisms to exchange electrons with solid surfaces (electrodes) and on the formation of a biofilm for an efficient transfer of electrons [7]. For instance, the presence of mixed cultures on anodic biofilms and the syntrophic relationships and interactions between them makes the degradation of complex substrates possible [8], which in turn makes the operation of BES more sustainable and resilient [9]. Therefore, a deeper understanding of the structure of anodic biofilms and the distribution of this biofilm on the anode, and the nature of the above mentioned interactions would undoubtedly help to improve the general performance of BES and allow a broadening of the range of potential substrates [10]. This interest in the microbiology of BES has gained a new momentum in the past years with the use of new methodologies such as high-throughput sequencing [11], which are proving to be very useful in identifying all the bacteria that make up the microbial community, thus helping to gain new insights on the role that microorganisms play in the whole BES performance.

1	The membrane is another key element in BES technology. Although it is possible to

2	operate BES in a membrane-less configuration (i.e. no ion exchange membrane is

3	interposed between the anode and the cathode), the use of membrane is vital for

4	instance to obtain high-purity hydrogen in microbial electrolysis cells (MEC) [12], to

5	recover nutrients (nitrogen, phosphorus, potassium, etc) [13] from nutrient-rich

6	substrates or to avoid any interference between the anodic and cathodic process (e.g.

7	to prevent oxygen from reaching the anode in microbial fuel cells, MFC). The few studies

8	that have tackled the effect of using real substrates on membrane performance and

9	durability [14][15] have shown that membrane fouling by microorganisms, extracellular

10	polymers and inorganic salts are the most important factors behind the observed

11	degradation in the BES performance due to the physical blockage of cation transfer that

12	may cause a decay in the current. Real substrates also have a significant influence on

13	the performance of BES, as they usually display low buffer capacity, low conductivity and

14	can contain complex organic compounds [16], all of which represent important

15	challenges in the scale-up of BES systems [2][17]. Recent works have made important

16	contributions to improve the applicability of real substrates in BES by, for instance,

17	enhancing the anodic biofilm by promoting a fermenting-exoelectrogenic consortium

18	[18], hindering the activity of undesired electron sinks [16] or optimizing the reactor

19	configuration [19].

20	In this paper we try to gain knowledge on how real substrates, such as pig slurry, affect

21	large scale BES. Rather than assessing their influence on BES performance (for which

22	there is a whole body of literature [16][20]) we put the focus on understanding their impact

23	on the membrane and the bioanode of two relatively large BES (16 L each) designed for

24	pig slurry valorization (hydrogen production and ammonia recovery). On the one hand,

25	we try to assess the role that hydrostatic and hydrodynamic phenomena play on the

26	development of anodic microbial communities after 100 days of batch operation. On the

27	other hand, we evaluate the ageing process of the membrane in terms of loss in ion

28	exchange capacity, trying to connect this deterioration with surface or internal structure

modifications. The existence of any spatial patterns of deterioration/modification in these elements is also assessed.

2. Materials and methods

2.1 Experimental setup and system operation

All experiments were conducted in two-chambered MEC reactors (MEC-1 and MEC-2) (Figure S1, supplementary information) made of polypropylene and built as previously described [21], with a total volume of 8 L per chamber. The anodes were made of 5 mm-thick graphite felt (Sigratherm®, Germany) with stainless steel current collectors, and the cathodes consisted of stainless steel mesh electrodes. The projected surface area of electrodes was 0.18 m^2, and carbon felt was pretreated according to [22]. The two chambers were separated by a cation exchange membrane (CMI7000, Membranes International, USA). Both MECs were inoculated and operated following identical procedures. Regarding inoculation, they were inoculated with digestate from a local Wastewater Treatment Plant, and operated in fed-batch mode at room temperature during the entire experimental period. Fed-batch cycle duration varied from ~2 days to ~5 days, until cathodic gas production (H_2) stoped. The reactors were fed using the liquid fraction of pig slurry (partially oxidized at the farm) as anolyte (and supplemented with acetate at a concentration of 0.2 g/L) and phosphate buffered saline (PBS) 0.1M as catholyte (pH=7). Both anolyte and catholyte are renewed in each batch and both were recirculated by NLAV peristaltic pumps (Dosiper, Spain) with a flow rate of 15 L·h^{-1}. MECs were connected in parallel to a power supply (PS 2000 B, Elektro-Automatik, Germany), and the applied voltage was set at 1 V between anode and cathode to optimize TOC removal and TN recovery (compared to lower voltage) without incurring in an excessive energy consumption that might probably result from using higher voltages. Each individual circuit contained a 0.5 Ω resistor to measure the voltage, from which the current was calculated using Ohm's law ($I = U·R^{-1}$), and it was recorded every 10 min using a data acquisition system (Keithley 2700, USA). Pig slurry was collected from the

1   slurry pits of a swine farm located at León (Spain). The pig slurry was pretreated in the

2   farm with aeration and sedimentation process. Samples were taken almost weekly and

3   stored at 4° C for <20 days.

4   Table 1. Characterization of pig slurry used as feedings in the MEC.

Parameter (Unit)	Pig slurry
COT ($g \cdot L^{-1}$)	2.61
Acetate ($mg \cdot L^{-1}$)	270
NT ($g \cdot L^{-1}$)	3.1
$N-NH_4^+$ ($g \cdot L^{-1}$)	3.1
Phosphate ($mg \cdot L^{-1}$)	37
Sulphate ($mg \cdot L^{-1}$)	42
Chloride ($mg \cdot L^{-1}$)	1950
TSS ($g \cdot L^{-1}$)	17.4
VSS ($g \cdot L^{-1}$)	7.6
% VSS	44
pH	7.9
Conductivity ($dS \cdot m^{-1}$)	26

5

6   After inoculation, both MECs were operated in fed-batch mode for a period of 78 days

7   that may further be subdivided into two phases: phase 1 (P1), with a duration of 38 days

8   where (total nitrogen) TN concentration in the fed was maintained at about 0.5 $g \cdot L^{-1}$ by

9   diluting pig slurry in tap water, and phase 2 (P2), with a duration of 40 days where TN

10   concentration was gradually increased up to 3 $g \cdot L^{-1}$ (by increasing the proportion of pig-

11   slurry in the feed) (Figure S2, supplementary material). This feeding pattern was

12   designed to favor the acclimation of microbial communities to high nitrogen loads.

13   Ammonium was collected within the catholyte. Due to the recalcitrant nature of the lignin-

14   carbohydrate complex contained in the pig-slurry [23], an acetate supplement of 0.2 $g \cdot L^{-1}$

15   was added to maintain current levels and avoid any deterioration in the performance

16   that could be attributable to degradable organic matter scarcity.

17   **2.2 Chemical analysis and calculation**

18   Liquid samples were taken from anolyte and catholyte at the beginning and end of each

19   batch cycle. Total organic carbon (TOC) and total nitrogen (TN) were determined by a

TOC multi N/C 3100 (Analytikjena, Germany). The pH and conductivity were measured using a pH meter GLP 21 (Crison Instruments, Spain) and a conductivity meter (TetraCon 325, WTW, Germany), respectively. Gas production in the cathode ~~MEC~~ was measured using a Milligascounter MGC-1 PMMA (Ritter, Germany), and the gas composition was determined using a gas chromatograph CP 3800 GC (Varian, USA) where the carrier gas was argon.

The nitrogen recovery efficiency was determined as the ratio between the amount of TN in the catholyte effluent and the amount of TN in the anolyte influent. The nitrogen transport rate was calculated as the amount of TN that crosses the membrane from the anolyte to the catholyte per day and per membrane surface area (m^2). Cathodic gas recovery, coulombic efficiency and energy recovery of the MEC were calculated as previously described [24].

2.3 Selecting sampling points on the anodic biofilm and the ion exchange membrane

As hydrostatic and hydrodynamic phenomena can affect both the anodic biofilm and the membrane properties generating spatial heterogeneity [25][26], sampling locations for both elements were selected taking into account the hydrostatic pressure due to the height of the water column (top, middle and bottom of the cell) and anolyte flow rate (high and low flow velocities) (Figure 1A). The hydrodynamic behaviour of the anolyte was simulated by means of computational fluid dynamics techniques (CFD) using the commercial code Fluent R16.0 (Ansys, Lebanon, USA). The flow was assumed to be incompressible, steady, homogeneous, adiabatic and Newtonian. K-epsilon was used as the turbulence flow model and the volume mesh contains about 0.38 million tetrahedral elements. The simulation was performed with a recirculation flow rate of 15 $L \cdot h^{-1}$. Model simulation results are presented as fluid velocity plots, where calibrated tones show fluid velocity (Figure 1B). As expected, the highest velocities (>100 $m \cdot h^{-1}$) were found in the

1 proximity of the inlet (E1/M1) and outlet (E6/M6) recirculation ports, while most of the

2 bulk liquid remained with relatively low velocities in the range between 0 and 15 $m \cdot h^{-1}$.
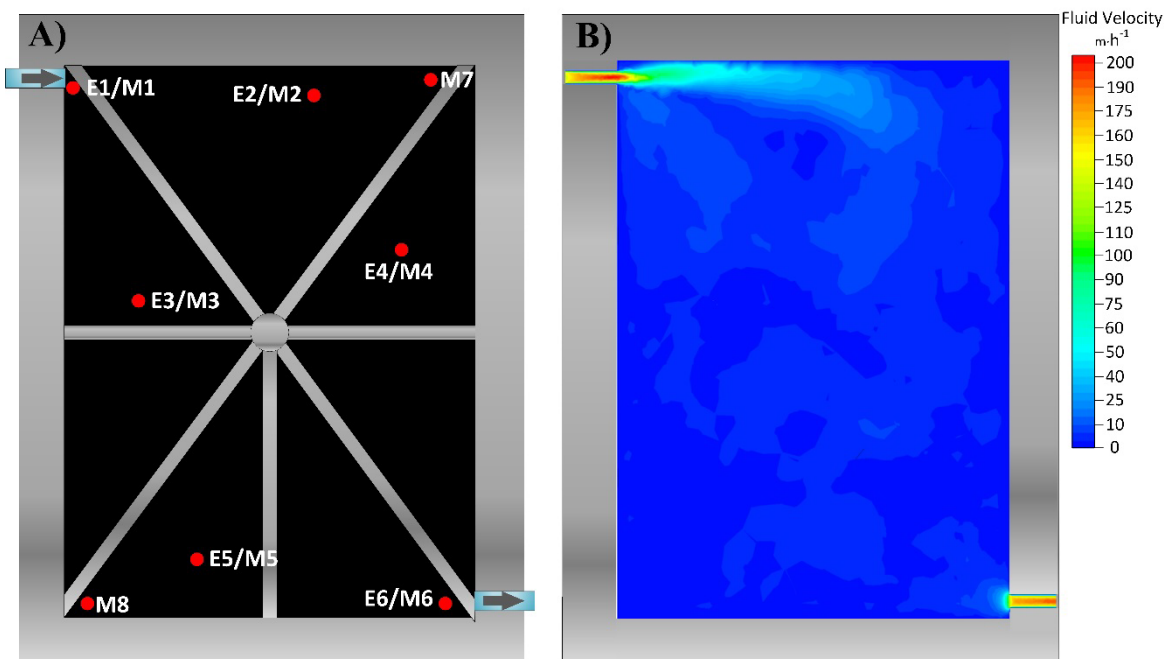
3

4 Figure 1. Schematic representation of the anode compartment indicating the electrode

5 (E1-E6) and membrane (M1-M8) sampling points (A), and the fluid velocity model (B).

6 **2.4 Membrane analysis**

7 Total membrane surface area was 0.18 m^2 and eight samples (of 2 cm^2 each) of the

8 membrane (M1-M8) of MEC-2 were analysed by several techniques: confocal and

9 scanning electron microscopies, thermogravimetry and ion exchange capacity titration.

10 Thermogravimetry analysis (TGA) of the cation exchange membranes was carried out

11 with a Thermogravimetric Analyzer SDT Q600 (TA Instruments, UK) in a temperature

12 range of 30 to 750 °C at the heating constant rate of 10 °C $\cdot min^{-1}$, under nitrogen

13 atmosphere. Ion exchange capacity (IEC) was determined by acid-base titration [27].

14 After the membrane was immersed in distilled water, it was soaked in a large volume of

15 1 M HCl for at least 24 hours (the solution was replaced three times to complete ion

16 exchange). Later, it was washed with distilled water to remove excess HCl and soaked

17 in 2 M NaCl solution for at least 24 hours to replace the protons by sodium ions (the

solution is replaced three times to ensure complete exchange). The different NaCl solutions were collected and then titrated with 0.1 M NaOH. The IEC titration of the membrane was calculated as the ratio between the number of fixed charges inside the ion exchange membrane (meq) and the dry weight of the measured membrane (g). The membrane samples were examined by the JSM-6480 LV (JEOL, Japan) scanning electron microscope (SEM). The samples were fixed in 2.5% glutaraldehyde solution in PBS for 2 hours at 4°C. When dry the membranes with ethanol were transferred into the chamber of the critical point dryer CPD 030 (Bal-Tec, Germany). Subsequently and prior to observation of the microstructure by SEM, the membranes were coated with a thin layer of gold in an EM ACE200 (Leica Microsystems, Switzerland). Elemental components of the inorganic salt precipitations in the membrane surface were analysed using an energy dispersive x-ray (EDX) INCA (Oxford Instrument, UK), which is integrated in the SEM equipment. Surface properties were analysed by Confocal Microscopy (CM) (LEICA DCM 3D dual model). CM provides a convenient means of acquiring 3D images of an object. The Leica DCM 3D dual system was used to measure the surface topography and calculate the surface roughness parameters. Images were taken with a confocal objective with a magnification of 10x and a numerical aperture (NA) of 0.50.

2.5 Microbial community analysis

Genomic DNA was extracted for the carbon felt electrode at different sampling points (E1-E6) in MEC-2 with the PowerSoil® DNA Isolation Kit (MoBio Laboratories Inc., Carlsbad, CA, USA), following the manufacturer's instructions. The entire DNA extract was used for the pyrosequencing of eubacteria *16S-rRNA* gene based massive library. The primer set used was 27Fmod (5`-AGRGTTTGATCMTGGCTCAG-3`) /519R modBio (5`-GTNTTACNGCGGCKGCTG-3`) [28]. The PCR conditions were described in S3, supplementary information. The obtained DNA reads were compiled in FASTq files for further bioinformatics processing. The following steps were performed using QIIME:

1 Denoising, using a Denoiser [29]. OTUs were then taxonomically classified using the

2 Ribosomal Database Project (RDP) Bayesian Classifier (http://rdp.cme.msu.edu) and

3 compiled into each taxonomic level with a bootstrap cutoff value of 80% [30]. Raw

4 pyrosequencing data obtained from this analysis were deposited in the Sequence Read

5 Archive (SRA) of the National Center for Biotechnology Information (NCBI).

6 Microbial richness estimators (S_{obs} and *Chao1*) and diversity index estimator (*Shannon*)

7 were calculated with the defined OTUs table (shared.file) using MOTHUR software,

8 version 1.35.1 at 3% distance level.

9 The quantitative analysis of Eubacteria population was analysed by means of

10 quantitative-PCR reaction (qPCR) using PowerUp SYBR Green Master Mix (Applied

11 Biosystems) in a StepOne plus Real Time PCR System (Applied Biosstems). The primer

12 set was 314F qPCR (5′-CCTACGGGAGGCAGCAG-3) and 518R qPCR (5′-

13 ATTACCGCGGCTGCTGG-3′).

14 3. **Results and discussion**

15 **3.1 MEC performance**

16
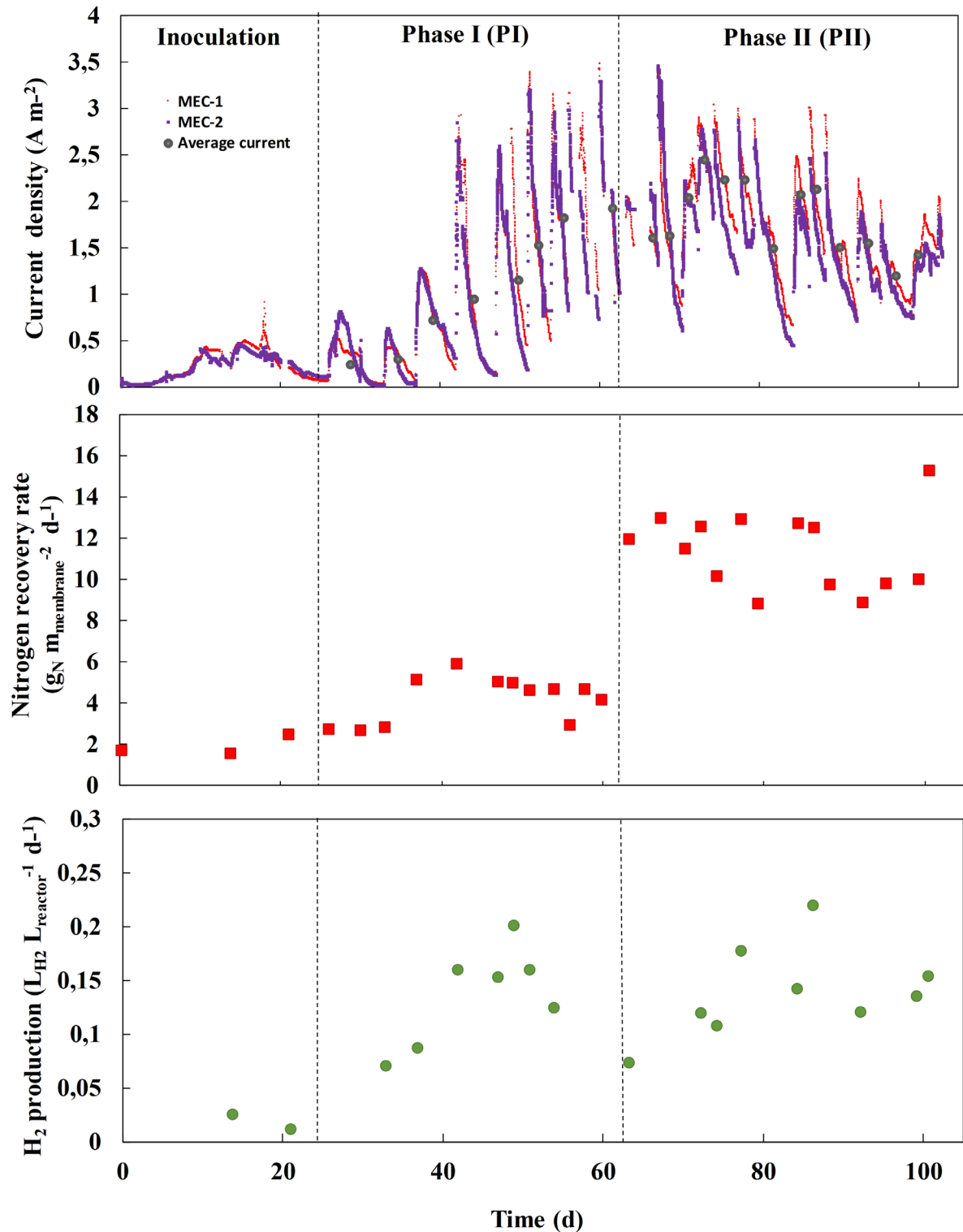
Figure 2. Operation of MEC-1 and MEC-2 with profiles for (A) current density, (B) nitrogen recovery rate and (C) hydrogen production rate.

Approximately 25 days after the inoculation (day 0), current density average values stabilized at 0.05 A·m⁻² (ampere per square meter of projected area of anode) (Figure 2). Current density profiles in both reactors followed similar trends showing a good

1   replicability (Figure 2). During phase P1 (see section 2.1 for a detailed description of the

2   operating phases), the current increased steadily with the number of batch cycles and

3   stabilized during P2 at ~1.75 A m^{-2}. Increasing the nitrogen content in the feed during P2

4   allowed the maximum ammonium transport rate through the membrane to increase from

5   5.9 gN·d^{-1}·m^{-2} during P1, to 15.3 gN·d^{-1}·m^{-2} in P which is in accordance with the results

6   obtained in previous works [31]. Ammonium concentration in the influent and effluent

7   streams of the MEC anode and ammonium removal efficiency are shown in Figure S2

8   (in the supplementary information). H_2 production (Figure 2) evolved along with current

9   production (this is especially noticeable during P1) achieving a maximum production rate

10   of 0.2 LH_2·$L^{-1}_{reactor}$·d^{-1} which is significantly lower than the 0.9 LH_2·$L^{-1}_{reactor}$·d^{-1} obtained by

11   Wagner et al. [20] using a similar substrate in a lab-scale (28 mL) MEC. However, the

12   presence of the membrane in our reactor allowed to produce hydrogen with a purity

13   always higher than 98 % (which compares with the 77% purity reported in the referred

14   work), with cathodic efficiencies of 84 ± 7 and 78 ± 16 % during P1 and P2, respectively.

15   The coulombic efficiencies were relatively low (in the range between 7% and 9%) as

16   expected from a complex substrate [32]. These results showed that despite the changes

17   in feeding pattern, the performance of both MECs was replicable and stable during the

18   whole operational period.

19   **3.2 Microbial community structure**

20   The development and spatial distribution of microbial communities present on the anodic

21   biofilm (points E1-E6 in Figure 2A) was studied by locally assessing biofilm richness,

22   diversity and microbial community composition.

23   **3.2.1 Assessing the anodic biofilm richness and diversity**

24   Total DNA was extracted from the carbon felt anode at the different sampling points

25   marked in Figure 1A to study the microbial community composition attached onto the

26   anode electrode at the end of the experiment. Between 43344 and 64444 effective

27   sequences in the six samples (E1-E6) were obtained. Each sample was rarefied to the

1 lowest number of sequences, with coverage values ranging from 98.3% to 99.1%, and

2 so they were a good representation of all the diversity that exists in the samples.

3 The similarity in the Shannon indexes as shown in Table 1 revealed the absence of big

4 differences in biofilm diversity along the anode surface. In contrast, the richness and the

5 number of sequences proved to be highly dependent on the sampling points, and the

6 differences found seem to be related to the fluid velocity (Figure 2). Indeed, the lowest

7 number of sequences were found in E1 and E6 (Table 1), where fluid velocity and thus

8 shear stress was more pronounced. More moderate velocities in E2 and E4 seem to

9 favor biofilm development, while those areas where fluid velocity got too low and

10 substrate diffusion might be hampered (E3 and E5), scored lower number of sequences.

11 Table 2. No. of sequences and OTUs, estimated richness (Chao1), diversity index (Shannon)

12 and sample coverage values for eubacterial operational taxonomic units (OTUs).

Sample	Nºseqs	sobs OTUs	Chao1		Shannon		Coverage (%)
			mean	(c.i.)*	mean	(c.i.)*	
E1	43,344	2065	2829	2696-2990	5.3	5.3-5.3	98.3
E2	61,209	2154	3080	2921-3272	4.9	4.8-4.9	98.7
E3	53,248	1961	2445	2350-2562	5.4	5.4-5.4	98.9
E4	64,444	2231	2598	2527-2688	5.5	5.4-5.5	99.1
E5	55,213	1954	2455	2356-2580	5.4	5.3-5.4	99.0
E6	49,200	1768	2122	2047-2217	5.3	5.3-5.4	99.0

13 *c.i. 95% confidence intervals

14

15 Regarding the richness indexes, the lowest values were found next to the outlet point

16 (E6), while both the flow inlet (E1) and the quadrant above (E2 and E4) showed a greater

17 number of different species, probably due to the input of the pig slurry loaded with a high

18 amount of microorganisms. Again those areas where the circulation of the anolyte

became limited (E3 and E5) showed relatively low richness, most likely as a result of the low mass transport rates in those areas.

The microbial community was also quantified by means of qPCR to corroborate the density of the biofilm at different anode positions. These results confirmed that fluid dynamics affect the abundance of eubacteria populations and therefore biomass as described above. The highest amount of *16S rRNA genes* were found in E2 (8.2×10^5 gene copy number g_{dw}^{-1} anode) and E4 (1.3×10^5 gene copy number g_{dw}^{-1} anode). However, the gene abundance in E3 (9.6×10^4 gene copy number g_{dw}^{-1} anode) and E5 (7.8×10^4 gene copy number g_{dw}^{-1} anode) was lower than those shown in E2 and E4. The sample taken from the points near to the effluent section (E6) showed the lowest gene abundance (4.3×10^4 gene copy number g_{dw}^{-1} anode), which coincides with the low number of sequences found here. These results were in agreement with other works [33] where the *16S rRNA* gene abundance gets reduced when the flow velocity is higher, and therefore the effect of the fluid velocity and shearing over the bacteria abundance in electrode biofilms is demonstrated.

3.2.2 Assessment of microbial populations stratification

The abundance of eubacteria community at phylum level (Table S4, supplementary information), showed that the two predominant phylum are *Firmicutes* and *Bacteroidetes* while *Proteobacteria*– being well known for playing an important role in extracellular electron transfer (EET) [34] – was present at a relatively lower abundance which is in agreement with [33]. Members of *Firmicutes* were also able to produce electricity in the anode of BES [35] and have been commonly detected in reactors treating pig slurry. These results showed that there are no major differences in composition or abundances of the microbial community at the different sampling points at phylum level. Notwithstanding, a distinct variation in the relative abundance at family level was clearly observed between electrode samples at different electrode points.

1 The *Clostridiaceae*, *Porphyromonadaceae*, *Eubacteriaceae* and *Anaerolineaceae*

2 families decreased in abundance from the top to the bottom of the electrode (Figure 3).

3 In contrast, *Ruminococcaceae*, *Erysipelotrichaceae* and *Synergistacea)* increased in

4 abundance towards the lower parts of the electrode.

5 The microbial community composition remained fairly stable in all samples, except for

6 four families *(Peptoniphilaceae*, *Enterococcaceae*, *Carnobacteriaceae* and

7 *Acholeplasmataceae)* which represented low abundances that are only identified in E1

8 and E2 sampling points.

9
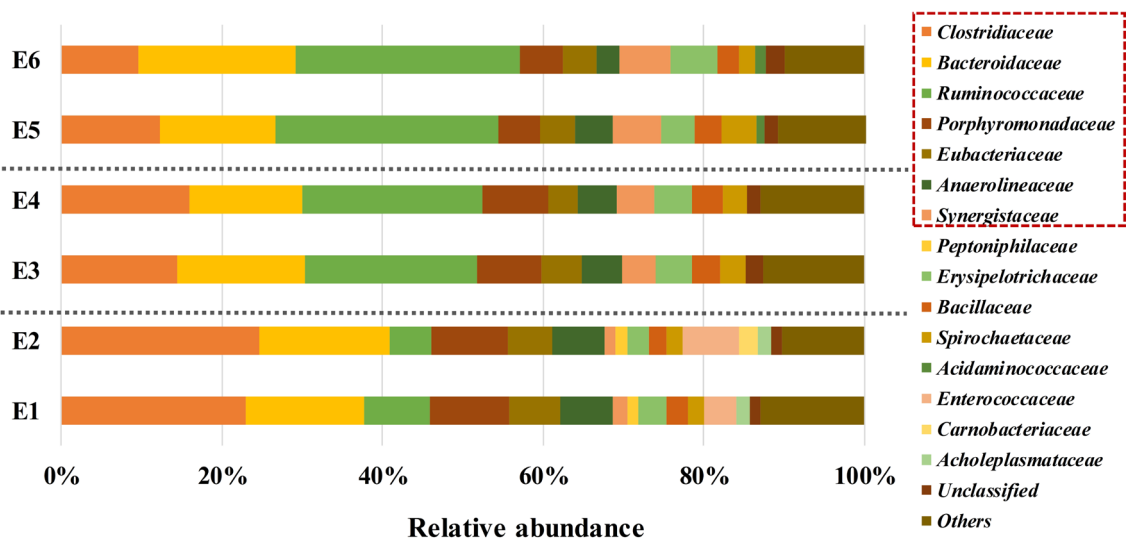
10 Figure 3. Taxonomic assignment of illumina data from eubacterial communities at different

11 sampling points at family level. Groups accounting for less than 1% of the total number of

12 sequences per sample are classified as "others".

13 Therefore, these results suggest that there was a vertical stratification of certain microbial

14 populations respective of their position in the electrode. This can be more clearly

15 observed in Figure 4, which represents three clusters that coincide with three heights in

16 the electrode: E1-E2 at the top, E3-E4 at the middle and E5-E6 at the bottom). Figure 4

17 also gives us an overview of the main genera identified in all samples at the end of the

18 experiments: members of *Acetivibrio*, *Clostridium*, *Proteiniphylum*, *Ruminococcus*,

19 *Eubacterium*, *Anaerofilum*, *Synergistetes*, *Bacteroides*, *Enterococcus* and *Bellilinea*

20 were the most representative in abundances above 7%. These genera belong to the

15

1   families that make the differences between the three clusters. Additionally, it can be

2   stated that electroactive bacteria, belonging mainly to *Proteobacteria and Firmicutes*

3   *Phyla* (*Pseudomonas, Sporomusa, Corynebacterium, Geobacter, Streptococcus,*

4   *Bacillus, Desulfovibrio* and *Acinetobacter),* were present in lower abundances in all of

5   our samples regardless of the position.

6   The best part of *Firmicutes* was *Clostridium* sp., becoming the most abundant genus in

7   our reactor (21%). Contrary, *Geobacter* sp. was in a low abundance (less than 1%).

8   *Geobacter* has previously been described as having competitive disadvantages relative

9   to *Clostridium* [36]. Anyway, despite the competition of certain microorganisms, the

10   presence of electroactive bacteria in all positions together with specific bacteria from

11   complex substrates makes a stable biofilm which is a key factor in maintaining the

12   performance in a long-term operation.

1
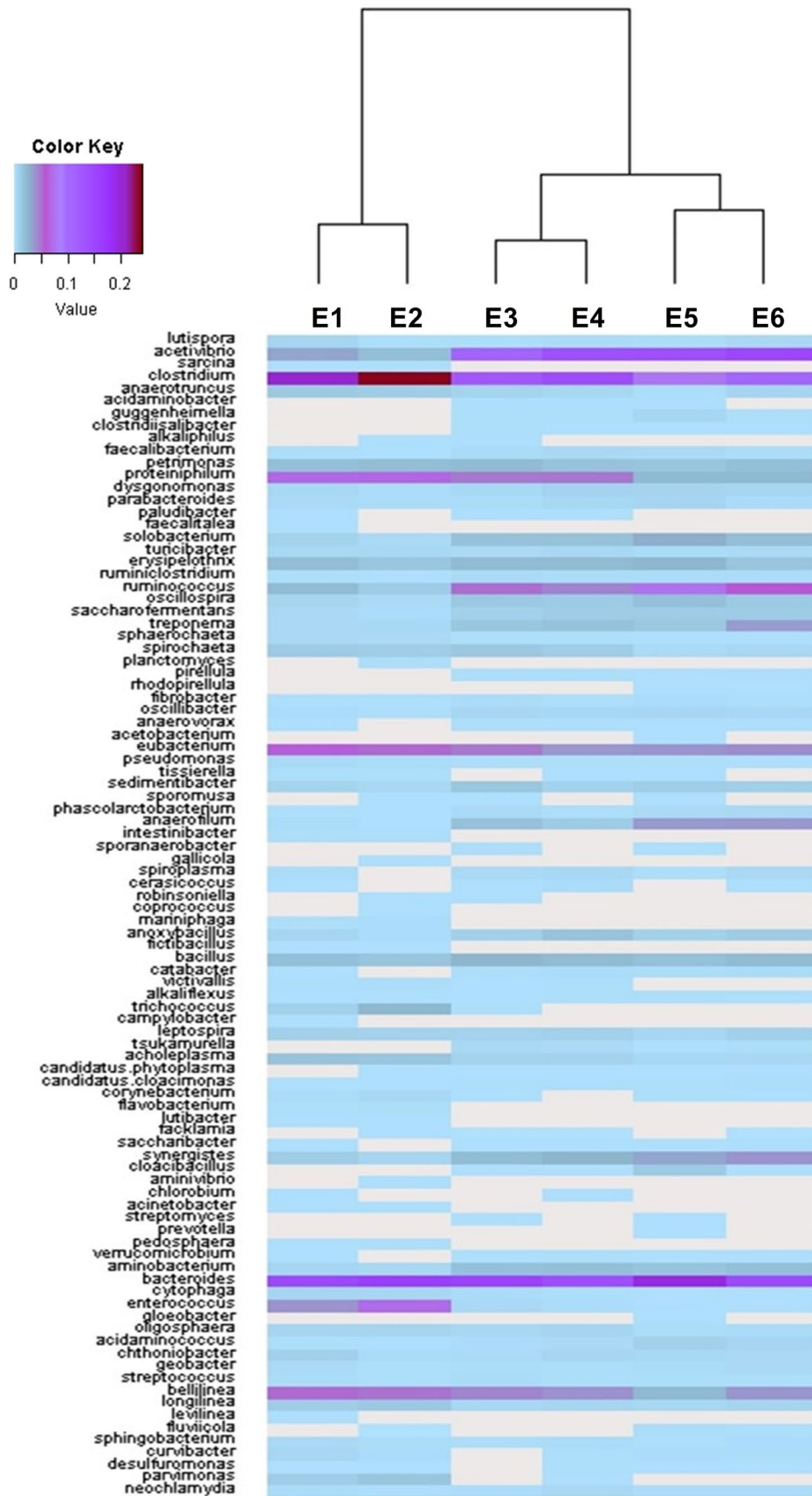
Figure 4. Heat map of the main dominate classified genera.

3.3 Assessment of membrane ageing

Membrane deterioration was evaluated based on results from ion exchange capacity (IEC), a parameter that represents the number of fixed charges inside the membrane per unit weight of dry polymer [37]. IEC has a definite impact on cell performance as it is intimately related to membrane electrical resistance: low IEC values usually translate into high electrical resistances and vice versa [38]. In our reactors, IEC underwent the highest deterioration (~22 % decrease) in samples M1 and M6 which were located at the inlet and outlet respectively, while the lowest deterioration was found in M7 (9%) (Table 2). In the rest of membrane samples (M2, M3, M4, and M5) IEC decreased by about 15%.

Table 3. IEC values and topography parameters: IEC (Ion Exchange Capacity), Ssk (Surface Skewness) and Sku (Surface Kurtosis)

| Membrane	IEC (meq/g)	Ssk (-)	Sku (-)
Blank	1.60	-1.22	63.66
M1	1.27	1.57	16.80
M2	1.39	1.56	17.47
M3	1.36	1.77	27.21
M4	1.37	4.08	43.05
M5	1.35	4.56	62.85
M6	1.23	1.49	22.77
M7	1.45	1.71	26.84
M8	1.34	2.05	25.16

This IEC deterioration can be attributed to either a modification of the internal structure of the membrane, to surface (bio-)fouling phenomena or both. The following sections are devoted to understanding to which extent they explain the observed loss in IEC.

3.3.1 Assessment of membrane structural deterioration

Internal membrane deterioration was assessed by means of themogravimetric analysis (TGA). Any decay in the properties of the membrane can be explained by either a

18

degradation of the structure of the membrane (polymer matrix) or of the sulfonic ($-SO_3H$)

groups [39], that play a determining role in cation exchange, or both. As shown in Figure

5, the membrane presented five significant thermal degradation zones. The first zone (I)

(below 100 °C) was attributed to the evaporation of water (thermal desolvation). The

second significant zone (II), occurring within an inflection temperature ranges between

150°C and 170 °C, was assigned to the loss of water molecules absorbed by $-SO_3H$

groups or adsorbed by the hydrogen-bonded to the membrane. The third zone (III),

between 300°C and 400 °C, corresponded to the loss of $-SO_3H$ groups (thermal

desulfonation) [40]. The fourth zone (IV), between 400°C and 490°C, was attributed to

the decomposition of the perfluoroether chains of the membrane [41]. Finally, the fifth

zone (V), above 500 °C, was assigned to the degradation of residual solvent from the

manufacturing process.

TGA derivative (DTGA) profiles in Figure 5 (and TGA profiles in Figure S5,

supplementary material) show a clear divergence between the blank membrane (virgin

membrane) and the used one. This deviation becomes more apparent in samples M1,

M2 and M7, where the peaks attributed to the thermooxidation of the polymer chain

increase and get displaced towards low temperatures. Moreover, the peak attributed to

the loss of $-SO_3H$ was more prominent there. Interestingly, these three samples belong

to the top of the reactor, an area that could be affected by an inadequate humidification

or lack of water at particular times that makes the membrane more brittle and fragile [42].

The rest of the membrane samples also presented some signs of degradation, but they

were less apparent.
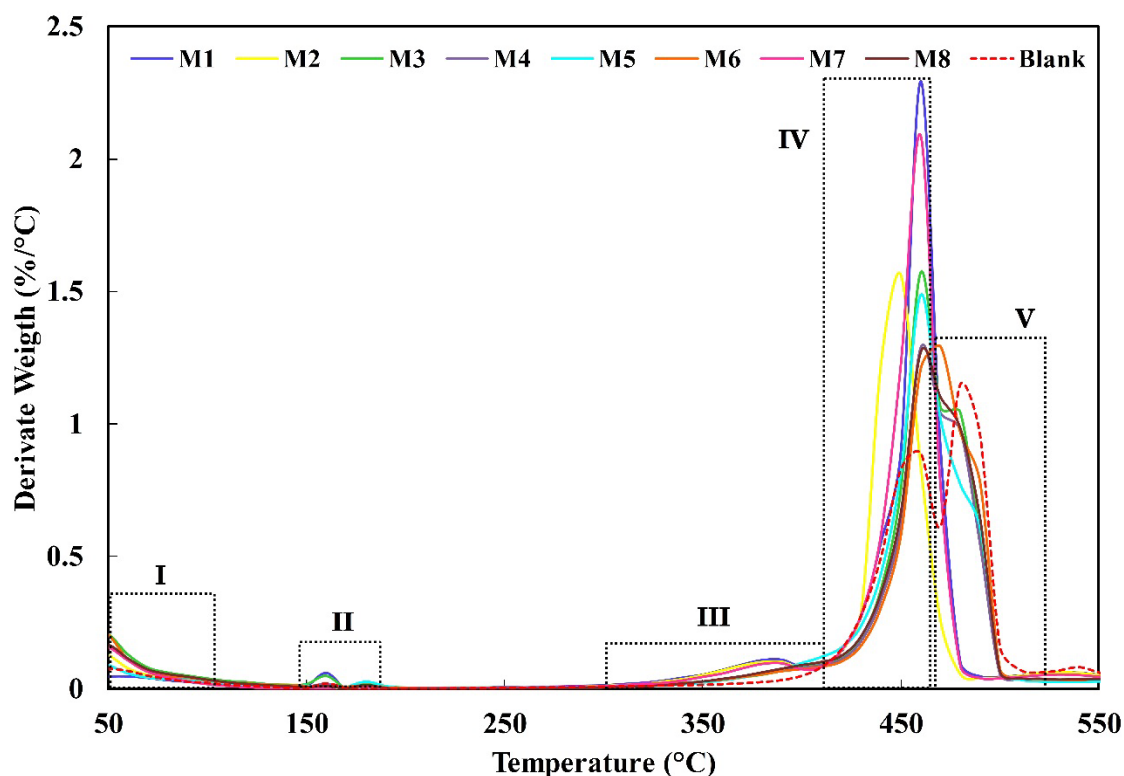
Figure 5. DTGA profiles of the different points of the membrane (this figure compares the thermal stability of the used membranes with respect to a blank membrane). Five significant zones are highlighted with Roman numerals: Zone I, evaporation of water; Zone II, loss of water molecules absorbed or adsorbed; Zone III, loss of –SO3H groups; Zone IV, decomposition of the perfluoroether chains; Zone V, degradation of the main chain.

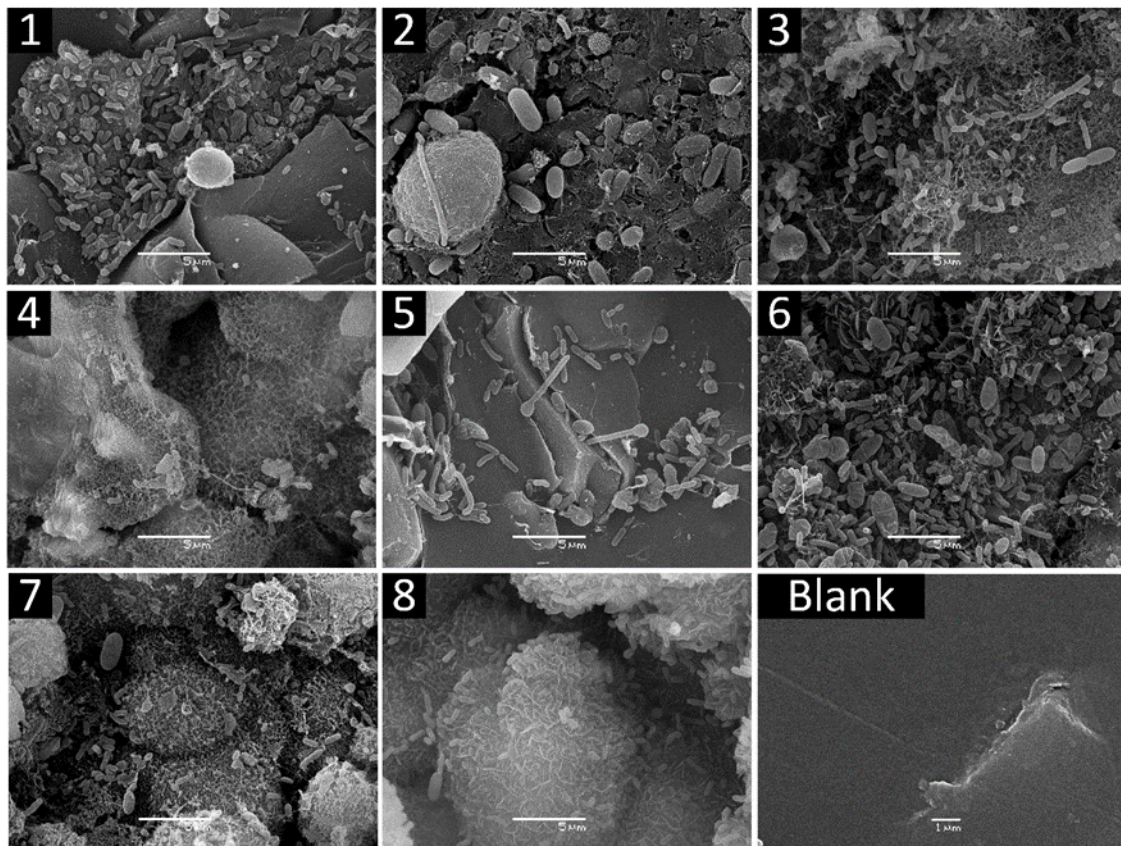### 3.3.2 Assessment of membrane surface modifications

Membrane biofouling represents an important issue in two-chambered configurations as a biomass layer can block the membrane pores, acting as a barrier to charges transport. SEM images revealed a strong attachment of microorganisms forming a biofilm embedded in the polymeric matrix on the anodic side of the membrane (Figure 6), and there appeared to be a certain correlation between membrane biofilm and anodic biofilm. Indeed, those regions of the membrane where the biofilm appeared to be broadly spread (M1 and M6 in Figure 6), corresponded to those anode samples which scored a lower number of sequences (E1 and E6, table 2). Conversely, membrane biofilm seems to be less dense in M5, where anodic biofilm was more developed (E5 in table 2). These

results suggest that where shear stress was hampering the development of an anodic biofilm (as a results of larger fluid velocity), the diffusion of the substrate to the membrane became facilitated, thus promoting biofilm formation in the membrane and vice versa. Low substrate contribution resulting from lower fluid velocity (Figure 2) could also explain the low biofilm formation in samples M7 and M8.

Figure 6. SEM images from different sample points from the membrane.

A more quantitative estimation of membrane surface modifications can be obtained by means of CM (Figure S6, supplementary material). This technique allows to quantify membrane topographic characteristics form the information provided by two parameters: surface skewness (Ssk) that represents the degree of symmetry of the surface heights about the mean plane, and surface kurtosis (Sku), which is equivalent to the peak density of the profile [43]. In general, more negative values of Ssk confirms the existence of a porous structure, while more positive correspond to a more even surface. Similarly, large values of Sku represent that protuberances on the surface have similar sizes.

1 The general trend for Sku and Ssk (Table 3) indicated that surface roughness wanes

2 with the use, leading to a topography with relatively more peaks and less valleys,

3 probably due to the biofouling of the holes. This became more apparent in samples M1,

4 M2 and M6 which coincided with those areas where the biofilm appeared to be more

5 spread as shown by SEM (Figure 6). Importantly, it was precisely in those samples

6 (specially in M1 and M6) where IEC suffers a greater decay, which reveals a certain

7 correlation between membrane biofouling and loss in membrane conductivity.

8 In addition to the biofouling observed on the anolyte side, the catholyte side of the

9 membrane also presented visible signs of deterioration as a uniform layer of salt

10 precipitations. EDX analysis showed that there are two types of precipitations (Figure

11 S7, supplementary material), one that was composed of oxygen, phosphorus and

12 calcium (calcium orthophosphate), and another type that was composed of oxygen,

13 phosphorus and magnesium (magnesium orthophosphate) that can be blocking charges

14 transfer. The presence of these precipitates can be explained by the fact that most of

15 the charge transport occurring through the CEM can be attributed to cations such as K^+,

16 Na^+, Ca^{2+}, Mg^{2+} and NH_4^+ rather than H^+ [44][45], that together with the phosphate from

17 the buffer solution, precipitated on the cathode side of membrane. Moreover, this

18 phenomenon can be also favored by the pH-splitting (between anode and cathode)

19 induced by the membrane, which tends to alkalinized the catholyte [46], leading to local

20 pH values slightly higher than 9 and thus promoting the formation of the precipitates

21 (despite a buffer solution was used as catholyte).

22

23   **3.4 Challenges and future perspectives**

24 The application scopes of MECs needs to be further expanded to make the most of this

25 versatile technology [47]. Combining nutrients recovery with hydrogen production in

26 MECs can help not only to offset the energy usage during organic wastes treatment [48],

27 but also to make MECs a more economically competitive and environmentally sound

28 technology. In this paper we have tried to shed some light on how two key elements of

MECs (the membrane and the anodic biofilm) behave during long term operation (>100 days) at pilot scale. Although membranes are not strictly necessary to produce hydrogen in MECs [2], they become an essential component in applications such as that examined in the present study. Our results suggest that despite the significant signs of ageing of the membrane, there was no visible deterioration in the performance of the reactor. Importantly, the membrane used in this research is designed to be used in conventional electrochemical systems. Thus, a decrease in the ion exchange capacity of 22% (as reported in this paper) may not be that critical in MECs as it is in other electrochemical devices, where the current densities can be several orders of magnitude above those usually found in bioelectrochemical systems. This observation may open the door for the development of more affordable membranes in which the electrochemical performance requirements are less demanding. In this regard, some suggestions have been put forward in a recent excellent review by Bakonyi et al.[44], showing that there is still a way to go through new designs and development such as, for example, modifying the composition and structure of the polymer.

The electrogenic biofilm that "catalyses" the anodic reaction represents another key element in MECs. During the scale-up process, as the dimensions of the anodes increase, the occurrence of heterogeneities within the biofilm becomes more likely, (as shown in this work), which can lead to bioanodes operating below optimal conditions in terms of current density. Using current collectors to make the anodic potential more homogeneous [21], controlling anode potential and/or substrate loading during the start-up [49,50], or modifying the biofilm–electrode interfaces [51], can be seen as suitable strategies to favour the development of a more homogenous biofilm.

Finally, the use of waste streams with high solids content represents another important challenge when scaling-up MECs. While pig slurry may *a priori* seem an unsuitable substrate, our results confirm that MECs can open up new perspectives for the valorization of this waste [20][52].Thus, and due to the large amounts of pig slurry produced globally each year [53], MECs would allow to recover ~$1.5 \cdot 10^6$ tons of NH_3 and

101,000 tons of H_2 per year and help to curb the energy usage in the fertilizers industry [19] .

4. Conclusions

Two double-chambered MECs were fed with pig slurry in fed-batch mode for 103 days to assess both membrane deterioration and the development of microbial anodic communities. Regarding the later, there seemed to be a vertical stratification of certain microbial populations. Results also confirm the mutualistic relationship between fermentative and electroactive bacteria in a MEC fed with a fermentable substrate and the importance of this relationship on stable MEC performance. Regarding the membrane, ion exchange capacity (a parameter intimately related to electrical resistance) seemed to be more affected by surface modifications than by internal structure (polymeric and sulphonic groups) degradation. The production of hydrogen and ammonia recuperation make this process a claim for circular economy.

References

[1]   Cecconet D, Molognoni D, Callegari A, Capodaglio AG. Agro-food industry wastewater treatment with microbial fuel cells: Energetic recovery issues. Int J Hydrogen Energy 2018;43:500–11. doi:10.1016/J.IJHYDENE.2017.07.231.

[2] Escapa A, Mateos R, Martínez EJ, Blanes J. Microbial electrolysis cells: An emerging technology for wastewater treatment and energy recovery. From laboratory to pilot plant and beyond. Renew Sustain Energy Rev 2016;55:942–56. doi:10.1016/j.rser.2015.11.029.

[3] Lai M-F, Lou C-W, Lin J-H. Improve 3D electrode materials performance on electricity generation from livestock wastewater in microbial fuel cell. Int J Hydrogen Energy 2018;43:11520–9. doi:10.1016/J.IJHYDENE.2017.06.047.

[4] Sivasankaran A, Sangeetha D. Influence of sulfonated SiO2 in sulfonated polyether ether ketone nanocomposite membrane in microbial fuel cell. Fuel 2015;159:689–96. doi:10.1016/J.FUEL.2015.07.002.

[5] Angioni S, Millia L, Bruni G, Tealdi C, Mustarelli P, Quartarone E. Improving the performances of Nafion™-based membranes for microbial fuel cells with silica-based, organically-functionalized mesostructured fillers. J Power Sources 2016;334:120–7. doi:https://doi.org/10.1016/j.jpowsour.2016.10.014.

[6] Rozendal RA, Hamelers HVM, Rabaey K, Keller J, Buisman CJN. Towards practical implementation of bioelectrochemical wastewater treatment. Trends Biotechnol 2008;26:450–9. doi:http://dx.doi.org/10.1016/j.tibtech.2008.04.008.

[7] Franks AE, Malvankar N, Nevin KP. Bacterial biofilms: the powerhouse of a microbial fuel cell. Biofuels 2010;1:589–604. doi:10.4155/bfs.10.25.

[8] Ichihashi O, Vishnivetskaya TA, Borole AP. High-Performance Bioanode Development for Fermentable Substrates via Controlled Electroactive Biofilm Growth. ChemElectroChem 2014;1:1940–7. doi:10.1002/celc.201402206.

[9] Borole AP, Tsouris C, Pavlostathis SG, Yiacoumi S, Lewis AJ, Zeng X, et al. Efficient Conversion of Aqueous-Waste-Carbon Compounds Into Electrons, Hydrogen, and Chemicals via Separations and Microbial Electrocatalysis. Front

Energy Res 2018;6:94. doi:10.3389/fenrg.2018.00094.

[10] Baranitharan E, Khan MR, Yousuf A, Teo WFA, Tan GYA, Cheng CK. Enhanced power generation using controlled inoculum from palm oil mill effluent fed microbial fuel cell. Fuel 2015;143:72–9. doi:10.1016/J.FUEL.2014.11.030.

[11] Rivalland C, Madhkour S, Salvin P, Robert F. Electrochemical and microbial monitoring of multi-generational electroactive biofilms formed from mangrove sediment. Bioelectrochemistry 2015;106:125–32. doi:10.1016/J.BIOELECHEM.2015.05.011.

[12] Guo K, Prévoteau A, Rabaey K. A novel tubular microbial electrolysis cell for high rate hydrogen production. J Power Sources 2017;356:484–90. doi:https://doi.org/10.1016/j.jpowsour.2017.03.029.

[13] Zou S, Qin M, Moreau Y, He Z. Nutrient-energy-water recovery from synthetic sidestream centrate using a microbial electrolysis cell - forward osmosis hybrid system. J Clean Prod 2017;154:16–25. doi:10.1016/J.JCLEPRO.2017.03.199.

[14] Köroğlu EO, Özkaya B, Denktaş C, Çakmakci M. Electricity generating capacity and performance deterioration of a microbial fuel cell fed with beer brewery wastewater. J Biosci Bioeng 2014;118:672–8. doi:10.1016/J.JBIOSC.2014.05.006.

[15] Çetinkaya AY, Köroğlu EO, Demir NM, Baysoy DY, Özkaya B, Çakmakçı M. Electricity production by a microbial fuel cell fueled by brewery wastewater and the factors in its membrane deterioration. Chinese J Catal 2015;36:1068–76. doi:10.1016/S1872-2067(15)60833-6.

[16] Lu L, Ren ZJ. Microbial electrolysis cells for waste biorefinery: A state of the art review. Bioresour Technol 2016;215:254–64. doi:10.1016/J.BIORTECH.2016.03.034.

1 [17] Logan BE. Scaling up microbial fuel cells and other bioelectrochemical systems.

2   Appl Microbiol Biotechnol 2010;85:1665–71. doi:10.1007/s00253-009-2378-9.

3 [18] Montpart N, Rago L, Baeza JA, Guisasola A. Hydrogen production in single

4   chamber microbial electrolysis cells with different complex substrates. Water

5   Res 2015;68:601–15. doi:http://dx.doi.org/10.1016/j.watres.2014.10.026.

6 [19] San-Martín MI. Bioelectrochemical Systems for Energy Valorization of Waste

7   Streams. In: Leicester DD, editor., Rijeka: IntechOpen; 2018, p. Ch. 8.

8   doi:10.5772/intechopen.74039.

9 [20] Wagner RC, Regan JM, Oh S-E, Zuo Y, Logan BE. Hydrogen and methane

10   production from swine wastewater using microbial electrolysis cells. Water Res

11   2009;43:1480–8. doi:10.1016/J.WATRES.2008.12.037.

12 [21] Escapa a., San-Martín MI, Mateos R, Morán a. Scaling-up of membraneless

13   microbial electrolysis cells (MECs) for domestic wastewater treatment:

14   Bottlenecks and limitations. Bioresour Technol 2015;180:72–8.

15   doi:10.1016/j.biortech.2014.12.096.

16 [22] Mateos R, Alonso RM, Escapa A, Morán A. Methodology for Fast and Facile

17   Characterisation of Carbon-Based Electrodes Focused on Bioelectrochemical

18   Systems Development and Scale Up. Materials (Basel) 2017;10.

19 [23] Shen J, Wang C, Liu Y, Hu C, Xin Y, Ding N, et al. Effect of ultrasonic

20   pretreatment of the dairy manure on the electricity generation of microbial fuel

21   cell. Biochem Eng J 2018;129:44–9. doi:10.1016/J.BEJ.2017.10.013.

22 [24] Baeza JA, Martínez-Miró À, Guerrero J, Ruiz Y, Guisasola A. Bioelectrochemical

23   hydrogen production from urban wastewater on a pilot scale. J Power Sources

24   2017. doi:10.1016/j.jpowsour.2017.02.087.

25 [25] Cecconet D, Bolognesi S, Molognoni D, Callegari A, Capodaglio AG. Influence

of reactor's hydrodynamics on the performance of microbial fuel cells. J Water Process Eng 2018;26:281–8. doi:10.1016/J.JWPE.2018.10.019.

[26] Vila-Rovira A, Puig S, Balaguer MD, Colprim J. Anode hydrodynamics in bioelectrochemical systems. RSC Adv 2015;5:78994–9000.

[27] Nayak V, Jyothi MS, Balakrishna RG, Padaki M, Deon S. Novel modified poly vinyl chloride blend membranes for removal of heavy metals from mixed ion feed sample. J Hazard Mater 2017;331:289–99. doi:10.1016/J.JHAZMAT.2017.02.046.

[28] Hassan M, Fernandez AS, San Martin I, Xie B, Moran A. Hydrogen evolution in microbial electrolysis cells treating landfill leachate: Dynamics of anodic biofilm. Int J Hydrogen Energy 2018;43:13051–63. doi:10.1016/J.IJHYDENE.2018.05.055.

[29] Chen Y, Rajagopala SV, Braun P, Tasan M, Cusick M. Rapidly denoising pyrosequencing amplicon reads by exploiting rank-abundance distributions. Nat Publ Gr 2010;7:668–9. doi:10.1038/nmeth0910-668b.

[30] Cole JR, Wang Q, Cardenas E, Fish J, Chai B, Farris RJ, et al. The Ribosomal Database Project: Improved alignments and new tools for rRNA analysis. Nucleic Acids Res 2009;37:141–5. doi:10.1093/nar/gkn879.

[31] Cerrillo M, Oliveras J, Viñas M, Bonmatí A. Comparative assessment of raw and digested pig slurry treatment in bioelectrochemical systems. Bioelectrochemistry 2016;110:69–78. doi:10.1016/j.bioelechem.2016.03.004.

[32] Pandey P, Shinde VN, Deopurkar RL, Kale SP, Patil SA, Pant D. Recent advances in the use of different substrates in microbial fuel cells toward wastewater treatment and simultaneous energy recovery. Appl Energy 2016;168:706–23. doi:10.1016/J.APENERGY.2016.01.056.

1   [33]   Vilajeliu-Pons A, Bañeras L, Puig S, Molognoni D, Vilà-Rovira A, Hernández-del

2   Amo E, et al. External Resistances Applied to MFC Affect Core Microbiome and

3   Swine Manure Treatment Efficiencies. PLoS One 2016;11:e0164044.

4   doi:10.1371/journal.pone.0164044.

5   [34]   Ishii S, Suzuki S, Norden-krichmar TM, Nealson KH, Sekiguchi Y, Gorby YA, et

6   al. Functionally Stable and Phylogenetically Diverse Microbial Enrichments from

7   Microbial Fuel Cells during Wastewater Treatment 2012;7.

8   doi:10.1371/journal.pone.0030495.

9   [35]   Wrighton KC, Agbo P, Warnecke F, Weber KA, Brodie EL, DeSantis TZ, et al. A

10   novel ecological role of the Firmicutes identified in thermophilic microbial fuel

11   cells. ISME J 2008;2:1146–56. doi:10.1038/ismej.2008.48.

12   [36]   Lewis AJ, Campa MF, Hazen TC, Borole AP. Unravelling biocomplexity of

13   electroactive biofilms for producing hydrogen from biomass. Microb Biotechnol

14   2018;11:84–97. doi:10.1111/1751-7915.12756.

15   [37]   Długołęcki P, Nymeijer K, Metz S, Wessling M. Current status of ion exchange

16   membranes for power generation from salinity gradients. J Memb Sci

17   2008;319:214–22. doi:https://doi.org/10.1016/j.memsci.2008.03.037.

18   [38]   Namdari M, Kikhavani T, Ashrafizadeh SN. Synthesis and characterization of an

19   enhanced heterogeneous cation exchange membrane via nanoclay. Ionics (Kiel)

20   2017;23:1745–58. doi:10.1007/s11581-017-2009-x.

21   [39]   Ghalloussi R, Garcia-Vasquez W, Chaabane L, Dammak L, Larchet C, Deabate

22   SV, et al. Ageing of ion-exchange membranes in electrodialysis: A structural and

23   physicochemical investigation. J Memb Sci 2013;436:68–78.

24   doi:10.1016/J.MEMSCI.2013.02.011.

25   [40]   Klaysom C, Ladewig BP, Lu GQM, Wang L. Preparation and characterization of

sulfonated polyethersulfone for cation-exchange membranes. J Memb Sci 2011;368:48–53. doi:10.1016/J.MEMSCI.2010.11.006.

[41] Wang F, Hickner M, Kim YS, Zawodzinski TA, McGrath JE. Direct polymerization of sulfonated poly(arylene ether sulfone) random (statistical) copolymers: candidates for new proton exchange membranes. J Memb Sci 2002;197:231–42. doi:https://doi.org/10.1016/S0376-7388(01)00620-2.

[42] Collier A, Wang H, Yuan XZ, Zhang J, Wilkinson DP. Degradation of polymer electrolyte membranes. Int J Hydrogen Energy 2006;31:1838–54. doi:https://doi.org/10.1016/j.ijhydene.2006.05.006.

[43] Stawikowska J, Livingston AG. Assessment of atomic force microscopy for characterisation of nanofiltration membranes. J Memb Sci 2013;425–426:58–70. doi:10.1016/J.MEMSCI.2012.08.006.

[44] Bakonyi P, Koók L, Kumar G, Tóth G, Rózsenberszki T, Nguyen DD, et al. Architectural engineering of bioelectrochemical systems from the perspective of polymeric membrane separators: A comprehensive update on recent progress and future prospects. J Memb Sci 2018;564:508–22. doi:10.1016/J.MEMSCI.2018.07.051.

[45] Harnisch F, Warmbier R, Schneider R, Schröder U. Modeling the ion transfer and polarization of ion exchange membranes in bioelectrochemical systems. Bioelectrochemistry 2009;75:136–41. doi:10.1016/J.BIOELECHEM.2009.03.001.

[46] Oliot M, Galier S, Roux de Balmann H, Bergel A. Ion transport in microbial fuel cells: Key roles, theory and critical review. Appl Energy 2016;183:1682–704. doi:10.1016/J.APENERGY.2016.09.043.

[47] Zhang Y, Angelidaki I. Microbial electrolysis cells turning to be versatile technology: Recent advances and future challenges. Water Res 2014;56:11–25.

1   doi:10.1016/J.WATRES.2014.02.031.

2   [48]   Zhang F, Li J, He Z. A new method for nutrients removal and recovery from

3   wastewater using a bioelectrochemical system. Bioresour Technol

4   2014;166:630–4. doi:10.1016/j.biotech.2014.05.105.

5   [49]   Ichihashi O, Vishnivetskaya TA, Borole AP. High-Performance Bioanode

6   Development for Fermentable Substrates via Controlled Electroactive Biofilm

7   Growth. ChemElectroChem 2014;1:1940–7. doi:10.1002/celc.201402206.

8   [50]   Lewis AJ, Borole AP. Adapting microbial communities to low anode potentials

9   improves performance of MECs at negative potentials. Electrochim Acta

10   2017;254:79–88. doi:10.1016/J.ELECTACTA.2017.09.085.

11 [51]   Alonso RM, San-Martín MI, Sotres A, Escapa A. Graphene oxide

12   electrodeposited electrode enhances start-up and selective enrichment of

13   exoelectrogens in bioelectrochemical systems. Sci Rep 2017;7:13726.

14   doi:10.1038/s41598-017-14200-7.

15 [52]   Sotres A, Cerrillo M, Viñas M, Bonmatí A. Nitrogen recovery from pig slurry in a

16   two-chambered bioelectrochemical system. Bioresour Technol 2015;194:373–

17   82. doi:10.1016/J.BIORTECH.2015.07.036.

18 [53]   Oenema O. Livestock production and manure management in EU-27.

19   ReUseWaste Kick off Meet., Copenhagen, Denmark: 2012.

20